Chapter 5

Solvation of Carbohydrates in 1,3-Dialkylimidazolium Ionic Liquids: Insights from Multinuclear NMR Spectroscopy and Molecular Dynamics Simulations

Igor D. Petrik, Richard C. Remsing, Zhiwei Liu, Brendan B. O'Brien, and Guillermo Moyna

West Center for Computational Chemistry and Drug Design and Department of Chemistry & Biochemistry, University of the Sciences in Philadelphia, 600 South 43rd Street, PA 19104-4495

Multinuclear NMR spectroscopy and molecular modelling represent two of the most important tools available to study the structure, solvation, and dynamics of ionic liquids and ionic liquid-based systems. This chapter showcases the application of these techniques to the investigation of carbohydrate solvation in 1,3-dialkylimidazolium ionic liquids. We show that when used in combination, ^{13}C and $^{35/37}Cl$ relaxation data, ^{1}H diffusion measurements, and molecular dynamics (MD) simulations can provide detailed information regarding this process at the molecular level. Our results point to a general solvation mechanism which is governed by the formation of hydrogen bonds between the ionic liquid anions and the hydroxyl group protons of the carbohydrate. Furthermore, both experimental and theoretical studies demonstrate that the interactions of the ionic liquid cation and the solutes are negligible. The application of similar approaches in the study of other relevant systems based on ionic liquids is briefly discussed.

Plechkova et al.; Ionic Liquids: From Knowledge to Application
ACS Symposium Series; American Chemical Society: Washington, DC, 2010.

Introduction

As evidenced by thousands of journal articles and an equally significant number of books devoted to their basic science and applications, ionic liquids have become increasingly important to the scientific community over the past decade. Originally recognised for their potential as "green" solvents, these low-melting organic salts have not only led to improvements in well established laboratory and industrial methods, but have also allowed for the development of new processes that were unattainable with traditional molecular solvents. Since it is possible to fine-tune their properties by modifying the chemical structure of their cation and anion components, ionic liquids can be in theory optimised to perform specific tasks. Consequently, these materials have found uses as battery electrolytes, lubricants, fuels, heat transport and storage fluids, and alternative media for synthesis, liquid-liquid extractions, and polymer processing, to mention a few examples. Many of these applications are described or cited in this and earlier volumes of the same series *(1)*.

The design of new ionic liquids tailored for particular applications requires knowledge of the interactions between the ionic liquid anions and cations and, more importantly, between these ions and solutes. A variety of techniques, including diffraction, spectroscopic, and computational methods, have been employed to investigate interionic interactions, dynamics, and solvation phenomena in these materials *(2-6)*. Among these, NMR spectroscopy and molecular dynamics (MD) simulations have found widespread use. Through the measurement of chemical shift perturbations *(7,8)*, nuclear Overhauser effects (nOes) *(9)*, relaxation rates *(10-13)*, and diffusion coefficients *(14,15)*, NMR experiments allow for the straightforward evaluation of the structure and dynamics of both the local and bulk environments of ionic liquids and ionic liquid-based solutions. While these experiments alone cannot explain certain phenomena atomistically, a variety of parameters obtained from NMR studies can be employed to validate results from MD simulations on these systems *(8,16)*. These experimentally supported models provide accurate atomic-level depictions of structure, dynamics, and intraionic and intermolecular interactions which are critical in the rational design and utilisation of ionic liquids and ionic liquid-based systems.

In this chapter, we showcase the application of some of these techniques to systems based on 1,3-dialkylimidazolium ionic liquids. In particular, we describe the use of ^{13}C and $^{35/37}Cl$ relaxation data, ^{1}H diffusion measurements, and MD simulations in the study of carbohydrate solvation in two imidazolium salts known to dissolve polysaccharides efficiently, 1-butyl-3-methylimidazolium chloride and 1-ethyl-3-methylimidazolium ethanoate ([C_4mim]Cl and [C_2mim][O_2CMe], Figure 1). As detailed in the following sections, results obtained using cellobiose as a model solute point to a general solvation mechanism in which the ionic liquids interact with carbohydrates through the formation of hydrogen bonds between the non-hydrated ionic liquid anions and the hydroxyl group protons of the sugar. In addition, our experimental and theoretical findings also confirm that the interactions between the ionic liquid cations and the carbohydrate are negligible.

The application of similar methodology to the study of other relevant ionic liquid-based systems is briefly discussed.

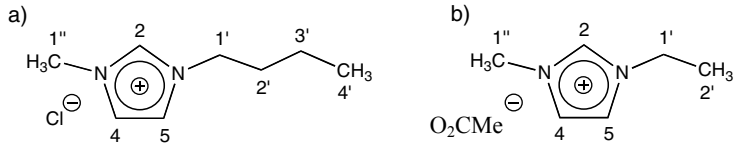

Figure 1. Structure and numbering of (a)[C_4mim]Cl and (b)[C_2mim][O_2CMe].

Materials and Methods

General

[C_4mim]Cl was prepared following reported procedures *(17)*. [C_2mim][O_2CMe] (97%) and D-cellobiose (98%) were purchased from Sigma-Aldrich (Milwaukee, WI). The ionic liquids were dried *in vacuo* (1×10^{-4} Torr) under vigorous stirring at 110 ºC for at least 16 h, and all materials were kept under vacuum until used. The absolute viscosities of the ionic liquids and ionic liquid solutions were determined using a ViscoLab 3000 temperature-controlled piston-type viscometer (Cambridge Applied Systems, Inc., Medford, MA).

NMR Experiments

Solutions of cellobiose in [C_4mim]Cl and [C_2mim][O_2CMe] were prepared by heating a mixture of the carbohydrate and the ionic liquid to 80 ºC with constant stirring. Upon complete dissolution, the samples were transferred to 5 mm NMR tubes that were then fitted with 60 μL co-axial inserts containing dmso-d_6 required for field-frequency lock. Samples of the neat ionic liquids were prepared analogously.

Longitudinal (T_1) relaxation data for the ^{13}C nuclei in $[C_4mim]^+$, $[C_2mim]^+$, and $[O_2CMe]^-$ ions were obtained with a standard ^{13}C-{^{1}H} inversion recovery (180º - t_d - 90º - Acq) pulse sequence, using eight t_d increments. The T_1 times were computed by fitting the raw data to exponential functions of the form:

$$I(t_d) = I_o \cdot (1 - 2 \cdot e^{-t_d/T_1})$$

where I_o and T_1 are the fit variables. $^{35/37}$Cl longitudinal relaxation measurements for the chloride ion were performed using an inversion recovery sequence in which the 90º read pulse was substituted by a 90º-90º-90º ARING pulse train to reduce acoustic ringing effects *(12)*. Twelve t_d increments were employed in this case, and the values of T_1 were also estimated using the equation shown above. When necessary, nOe factors for ^{13}C nuclei of the ionic

liquid ions were computed from the ratio of the ^{13}C-{^{1}H} signal area recorded with continuous decoupling relative to that obtained using inverse-gated decoupling *(18)*. Experiments for the neat ionic liquids were performed in 10 ºC increments at temperatures ranging from 40 to 90 ºC for [C_4mim]Cl and 30 to 80 ºC for [C_2mim][O_2CMe]. Measurements for [C_4mim]Cl solutions were carried out at 90 ºC, and at 80 ºC in the case of [C_2mim][O_2CMe] solutions. It is worth noting that although its melting point is approximately 70 ºC *(2,17)*, [C_4mim]Cl and its solutions behave as supercooled fluids and remain liquid below this temperature for prolonged periods.

Diffusion coefficients for ions in the neat ionic liquids and ionic liquid/carbohydrate solutions were obtained using the ^{1}H-detected PFG-STE sequence 90º - G - 90º - Δ - 90º - G - Acq *(19)*, where Δ is the diffusion time and G represents a bipolar z-gradient block of the form G_{+z} - 180º - G_{-z} with overall duration δ and strength g *(20)*. For each measurement, a total of 16 data points were recorded by varying the gradient strength linearly while keeping the Δ and δ diffusion parameters constant. Self-diffusion coefficients (D) were estimated by fitting the ^{1}H signal intensity versus gradient strength to mono-Gaussian curves of the form *(21)*:

$$I(g) = I_o \cdot e^{-\gamma^2 g^2 \delta^2 D \cdot (\Delta - \delta/3)}$$

where I_o and D are the fit variables, γ represents the ^{1}H gyromagnetic ratio, and the remaining parameters were previously defined. The self-diffusion coefficient for any given ion was computed as the average of the D values obtained for all its protons. Diffusion measurements were carried out in 10 ºC increments at temperatures ranging from 40 to 100 ºC for [C_4mim]Cl and from 30 to 90 ºC for [C_2mim][O_2CMe] solutions.

All experiments were carried out on a Bruker AVANCE 400 NMR spectrometer equipped with 5 mm BBO and QNP z-gradient shielded probes, operating at ^{1}H, ^{13}C, ^{35}Cl, and ^{37}Cl frequencies of 400.13, 100.61, 39.21, and 32.64 MHz, respectively.

Simulation Details

MD simulations were performed employing the CM3D software package and the OPLS-AA force field with optimised van der Waals parameters for the chloride ion described earlier *(8,22-24)*. Partial charges for cellobiose, [C_4mim]Cl, and [C_2mim][O_2CMe] were computed from fits to their electrostatic potentials (ESPs) derived from *ab initio* calculations at the B3LYP/6-311+G* level of theory *(24)*. The initial configurations of all systems were obtained from previously equilibrated [C_4mim]Cl and [C_2mim][O_2CMe] simulation boxes. The cellobiose solutions were created by patching sugar molecules to the sides of the ionic liquid boxes until the correct concentration was obtained. In the case of the 5 wt% cellobiose solutions discussed below, a total of six sugar molecules were required in both cases. Periodic boundary conditions were employed, using the Ewald method to treat long-range electrostatic interactions

(25,26). The reversible reference system propagator algorithm (r-RESPA) with time steps of 0.5 and 2 fs was employed to evaluate short-range intramolecular forces and long-range interactions, respectively *(27)*. The systems were first equilibrated in the canonical ensemble (NVT) for 1 ns, followed by period of a 1 to 2 ns in the isothermal-isobaric ensemble (NPT) required to stabilise their densities. After an additional 1 ns equilibration period in the NVT ensemble, 10 ns production runs used in the analyses discussed below were performed under the same conditions. Simulations of $[C_4mim]Cl$ and $[C_2mim][O_2CMe]$ solutions were carried out at 363.15 and 353.15 K, respectively.

3. Results and Discussion

NMR Studies of Ionic Liquid/Cellobiose Systems

As we have recently reported, the relaxation of NMR-active nuclei in an ionic liquid depends on the dynamics of both ions and their interactions with solutes. In the case of imidazolium chlorides, the marked variation in the $^{35/37}Cl$ relaxation parameters with changes in the environment of the chloride ion makes these quadrupolar nuclei ideal to investigate sugar/ionic liquid solutions *(12,28)*. As a matter of fact, the dependency of $^{35/37}Cl$ transverse (T_2) relaxation times with carbohydrate concentration allowed us to establish that the solvation of sugars in $[C_4mim]Cl$ occurs through the formation of hydrogen bonds between the chloride ion and the solute hydroxyl group protons *(12)*. While the concentration dependency of the relaxation times of the ethanoate carbons is not expected to be as marked as that of the anions in imidazolium chloride salts, a similar approach should also be suitable to study $[C_2mim][O_2CMe]$/carbohydrate solutions.

We first investigated longitudinal relaxation times as a function of temperature and in the absence of solutes. Results for selected carbons of the $[C_4mim]^+$ and $[C_2mim]^+$ ions are presented in Figure 2. For $[C_4mim]^+$, the T_1 minima observed for the imidazolium ring carbons, C-1', and C-1" indicate that these nuclei transition from the extreme narrowing ($\omega_o \tau_c < 1$) to the diffusion limit ($\omega_o \tau_c > 1$) relaxation regime at ~70 ºC, Figure 2(a). Due to their higher mobility, the remaining butyl chain carbons fail to undergo this transition in the range of temperatures studied. In the case of $[C_2mim]^+$, all carbons remain in the extreme narrowing regime, Figure 2(b).

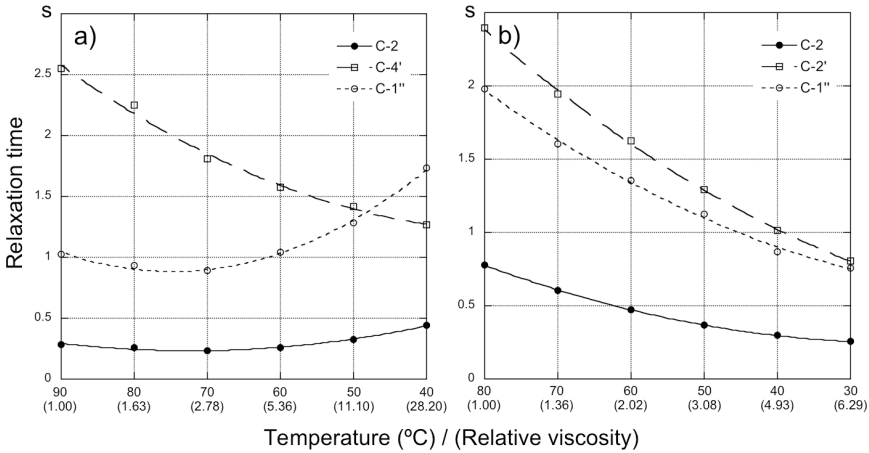

Figure 2. ^{13}C T_1 relaxation as a function of temperature for (a) C-2, C-4', and C-1" in [C_4mim]Cl, and (b) C-2, C-2', and C-1" in [C_2mim][O_2CMe].

Due to the smaller size of the ethyl side chain, the C-2' and C-1" carbons of this cation have similar mobilities. Overall, and in agreement with previous NMR and molecular dynamics simulation studies on analogous systems *(11,13)*, the temperature dependency of the ^{13}C relaxation rates for both imidazolium cations reflects the variations observed in the viscosities of the neat ionic liquids. Longitudinal relaxation data as a function of temperature for the anions for the two ionic liquids are presented in Figure 3. The pronounced increase in the T_1 times with rising temperature also correlates with changes in viscosity and is consistent with a weakening of interionic interactions *(12)*. It is also worth noting that in the range of temperatures considered, the anions of both ionic liquids remain in the extreme narrowing relaxation regime. This is evidenced by the fact that the chloride ion in [C_4mim]Cl has virtually indistinguishable T_1 and T_2 values, and that no T_1 minima are observed for the carbons of the ethanoate ion *(18)*. Based on these results, carbohydrate dissolution in [C_4mim]Cl and [C_2mim][O_2CMe] was studied at 90 and 80 ºC, respectively. All nuclei in the neat ionic liquids are in the extreme narrowing region at these temperatures, and thus pronounced changes in relaxation rates as a function of concentration are likely to indicate specific ionic liquid-solute interactions.

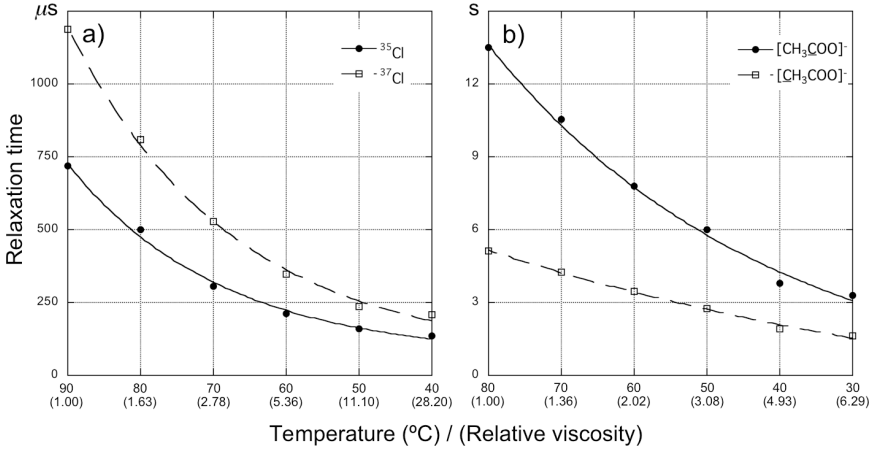

Figure 3. Temperature dependence of the $^{35/37}$Cl T_1 relaxation of the chloride ion in (a) [C_4mim]Cl, and (b) ^{13}C T_1 for the carbonyl and methyl carbons of the [O_2CMe]$^-$ ion in [C_2mim][O_2CMe].

As shown in Figure 4, there are only slight variations in the longitudinal relaxation of the carbons in both ionic liquid cations as a function of cellobiose content. In all cases, the changes in T_1 times over the whole concentration range are comparable with those observed upon varying the temperature of the neat ionic liquids by 10 ºC or less, and can be rationalised satisfactorily on the basis of changes in solution viscosity.

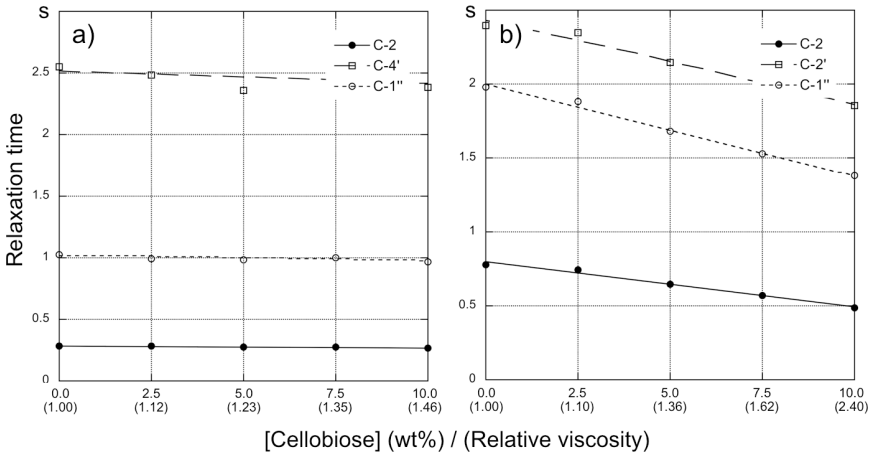

Figure 4. ^{13}C T_1 relaxation versus cellobiose concentration for C-2, C-4', and C-1" in (a)[C_4mim]Cl, and (b) C-2, C-2', and C-1" in [C_2mim][O_2CMe].

Conversely, the relaxation parameters of the ionic liquid anions are strongly influenced by the presence of sugars. For [C_4mim]Cl solutions, the changes in the longitudinal relaxation rates of the chloride ion as a function of carbohydrate

concentration are vastly larger than those expected based on the variation of the solution viscosity alone, Figure 5(a). For example, the T_1 times for the anion in 10 wt% cellobiose solutions in [C_4mim]Cl at 90 ºC, which has a viscosity of 112.3 cP, are considerably lower than in the neat ionic liquid at 40 ºC, which has a viscosity of 1716.0 cP. These large changes in the $^{35/37}$Cl relaxation parameters point to the disruption of the spherical symmetry around the quadrupolar nuclei, and are consistent with the formation of hydrogen bonds between the chloride ions and the carbohydrate hydroxyl group protons *(12)*. Although less pronounced, the dependency of the T_1 times of the ethanoate carbons with sugar concentration in [C_2mim][O_2CMe] solutions at 80 ºC is also clear, Figure 5(b).

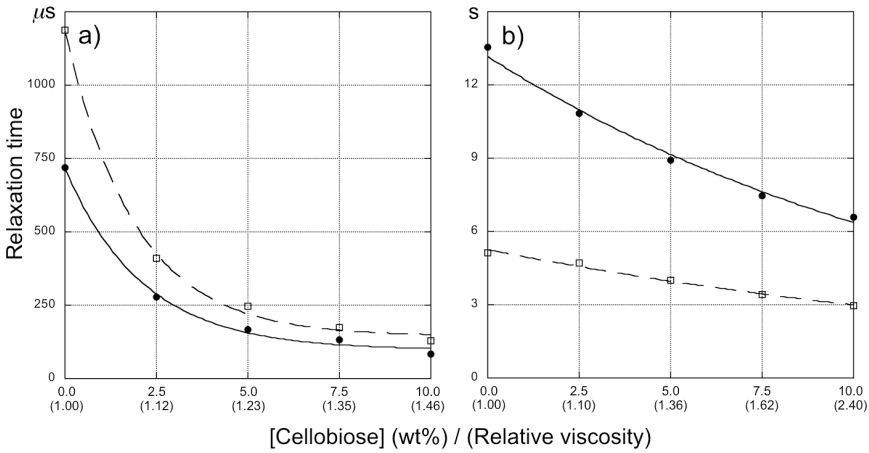

Figure 5. $^{35/37}$Cl T_1 relaxation for the chloride ion in (a)[C_4mim]Cl, and (b) ^{13}C T_1 relaxation times for the carbonyl and methyl carbons of the [O_2CMe]$^-$ ion in [C_2mim][O_2CMe] as a function of cellobiose concentration.

Further analysis of the ^{13}C and $^{35/37}$Cl relaxation data can provide detailed information regarding changes in the mobilities of the ions in both ionic liquids as a function of cellobiose concentration. The measured longitudinal relaxation times are the combination of a variety of relaxation processes *(18)*. These include, for example, dipolar interactions (R_1^D), chemical shift anisotropy (R_1^{CSA}), and quadrupolar coupling (R_1^Q):

$$\frac{1}{T_1} \equiv R_1 = R_1^D + R_1^{CSA} + R_1^Q + \ldots$$

In the case of protonated carbons, which applies to [C_4mim]$^+$ and both ions in [C_2mim][O_2CMe], R_1^D and R_1^{CSA} dominate. The two are related to the correlation time (τ_c) of the nuclei under scrutiny by the following expressions *(18)*:

$$R_1^D = \frac{N_H}{40} \cdot \frac{\gamma_C^2 \gamma_H^2 \mu_o^2 \hbar^2}{r_{CH}^6} \cdot \left(\frac{\tau_c}{1+(\omega_C - \omega_H)^2 \tau_c^2} + \frac{3\tau_c}{1+\omega_C^2 \tau_c^2} + \frac{6\tau_c}{1+(\omega_C + \omega_H)^2 \tau_c^2} \right)$$

$$R_1^{CSA} = \frac{1}{15} \cdot \gamma_C^2 B_o^2 \Delta\sigma^2 \cdot \left(\frac{2\tau_c}{1+\omega_C^2 \tau_c^2} \right)$$

N_H represents the number of attached protons and r_{CH} the C-H bond distance, μ_o is the permeability of vacuum, γ_C and γ_H are the gyromagnetic ratios of ^{13}C and ^{1}H and ω_C and ω_H their Larmor frequencies, respectively, $\hbar$ is the reduced Planck constant, B_o is the spectrometer magnetic field, and $\Delta\sigma$ is the chemical shift anisotropy of the nucleus under consideration. The τ_c values for protonated carbons in [C_4mim]Cl and [C_2mim][O_2CMe] solutions can be determined using the experimental ^{13}C T_1 data as input for these equations following the approach of Carper and coworkers *(11,13)*.

As stated earlier, the relaxation of the chloride ion in [C_4mim]Cl solutions is dominated by R_1^Q, which can also be expressed as a function of the correlation time of the anion *(18)*:

$$R_1^Q = \frac{1}{10} \cdot \left(1 + \frac{\eta^2}{3}\right) \cdot \left(\frac{e^2 Qq}{\hbar}\right) \cdot \tau_c$$

In this equation, η represents the assymetry parameter and $e^2Qq / \hbar$ the quadrupole coupling constant. These parameters have been recently reported for the chloride ion ^{35}Cl isotope in solid [C_4mim]Cl *(29)*, and they could in principle be used in the estimation of τ_c from experimental T_1 data. However, the changes in τ_c values measured in the ionic liquid/cellobiose solutions relative to those obtained for the neat ionic liquids are better suited to investigate changes in the mobility of the ions. This not only circumvents the need to compute correlation times in the case of the chloride ion, but also allows for clear comparisons of the variations in the mobilities of cations versus anions as a function of solute concentration.

As shown in Figure 6, the changes in τ_c as a function of sugar concentration are modest and comparable for all carbons in both imidazolium ions. Indeed, there is virtually no variation in the correlation times of the [C_4mim]Cl carbons. This not only indicates that the rotational mobilities of different regions of the cations are affected similarly by the presence of cellobiose, but is consistent with a lack of strong interactions between the cation and the carbohydrate. On the other hand, the variation of the τ_c values of the ethanoate ion methyl carbon and chloride ion reveals that the reorientation rate of the anions decreases sharply with increasing sugar concentration. In [C_2mim][O_2CMe] solutions, the tumbling rate of the anion decreases nearly twice as much as that of the cation when the concentration of cellobiose increases, while for [C_4mim]Cl solutions the change in the rotational mobility of the anion is nearly eight times larger than that observed for the cation. These results agree well with the preliminary conclusions derived from raw longitudinal relaxation data presented earlier, and

provide further evidence regarding the presence of specific interactions between the ethanoate ion and the sugar solute.

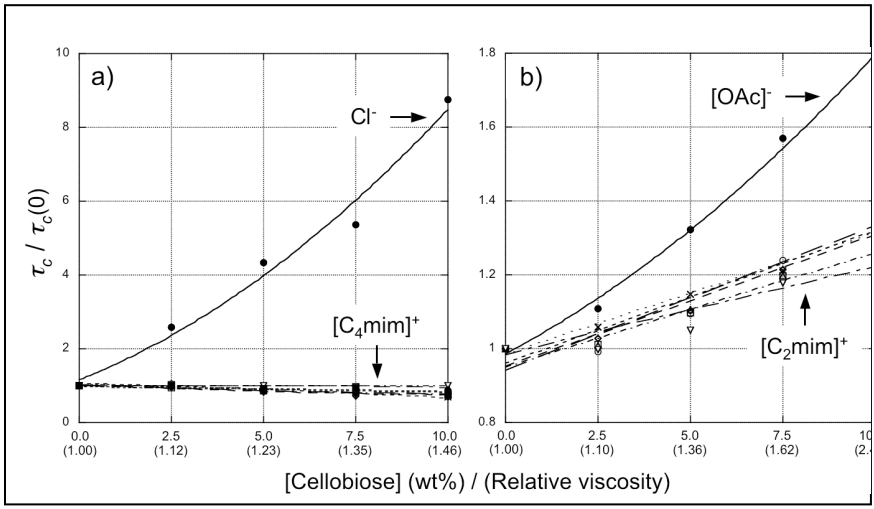

Figure 6. Relative variation in the τ_c values of nuclei in (a) [C_4mim]Cl and (b) [C_2mim][O_2CMe] as a function of cellobiose concentration.

Additional information regarding the effects of the sugar on the dynamics of the ionic liquid ions can be obtained by studying variations in their translational mobility *(15,16,30,31)*. This was done through the estimation of the self-diffusion coefficients of the $[C_4mim]^+$, $[C_2mim]^+$, and $[O_2CMe]^-$ ions as a function of temperature in the neat ionic liquids, as well as in 5 and 10 wt% cellobiose ionic liquid solutions (Figure 7). The relatively high viscosities of these systems lead to short ^{1}H T_2 times, and thus PFG-STE techniques were employed to carry out all measurements (*16*). Regardless of the method, the fast transverse relaxation of $^{35/37}$Cl nuclei precludes the estimation of the anion self-diffusivity in [C_4mim]Cl solutions using this or related techniques.

Not surprisingly, there is an inversely proportional relationship between the self-diffusivity of the cations and the viscosity of the neat ionic liquids, with $D_{[C2mim]+} >> D_{[C4mim]+}$. In the case of [$C_2$mim][$O_2$CMe], it is worth noting that the smaller ethanoate ion diffuses slower than the imidazolium cation. This behaviour has been observed for other ionic liquids, and suggests that the anions do not diffuse as isolated species but as part of larger ion aggregates *(30,31)*. Together with the increase in the viscosity of the systems, there is a substantial drop in the diffusion coefficients of all species as sugars are dissolved in the ionic liquids. In [C_2mim][O_2CMe] solutions, the diffusion of the ethanoate ion is affected more than that of the imidazolium cation by the dissolved carbohydrates. However, the differences are minimal and considerably smaller than those observed through analysis of ^{13}C relaxation data. This is not unexpected considering that even when their local mobility may be affected

differently by their interactions with carbohydrates (*vide supra*), anion and cation co-migration is required to maintain the charge balance of the systems.

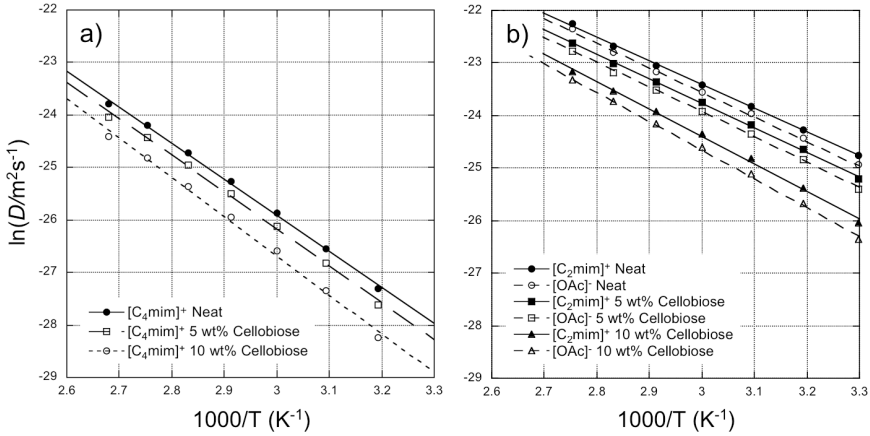

Figure 7. Arrhenius plots for the (a) $[C_4mim]^+$, (b) $[C_2mim]^+$ and $[O_2CMe]^-$ ions in the neat ionic liquids, as well as their 5 and 10 wt% cellobiose solutions.

MD Simulations of Ionic Liquid/Cellobiose Systems

We and others have recently employed MD simulations to investigate carbohydrate dissolution in imidazolium ionic liquids *(24,32,33)*. The results summarised in these reports, which considered exclusively $[C_4mim]Cl$ and $[C_1mim]Cl$, were in good agreement with NMR studies and corroborated that sugar solvation is governed by hydrogen bonding between the ionic liquid chloride ion and the solute hydroxyl groups. Since the results presented in the previous section of this chapter indicate that the process is analogous for chloride and ethanoate anions, we here extend our MD studies to $[C_2mim][O_2CMe]$/cellobiose solutions. In addition, we pay considerable attention to potential interactions between the ionic liquid cations and the solute, as these have been suggested to be of importance in some of the previous studies *(32,33)*. While MD simulations were carried out for all the solutions investigated by NMR, the results obtained for the 5 wt% ionic liquid/cellobiose solutions are representative and we limit our analyses to these systems.

Figure 8a shows the radial distribution functions (RDFs) between the sugar primary and secondary hydroxyl group protons and the chloride ion in the $[C_4mim]Cl$/cellobiose system. There is a prominent peak in the OH···Cl RDFs, or $g_{OH\cdots Cl}(r)$ functions, centred at 1.85 Å which indicates a strong interaction between the chloride ion and the hydroxyl protons. Similarly, analysis of the angular distribution functions (ADFs) for the O–H···Cl angle shows a strong maximum centred at ~170°, Figure 8(b). This distance and angle combination are in the ideal hydrogen bonding range, and thus our results clearly indicate the presence of hydrogen bonds between the hydroxyl protons and the chloride ion.

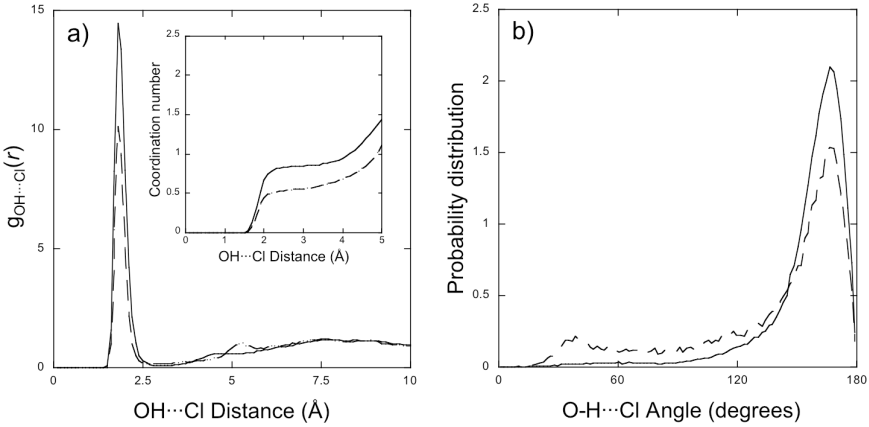

Figure 8. (a) OH···Cl RDFs and coordination numbers, and (b) O–H···Cl ADFs for the [C_4mim]Cl/cellobiose system. Results for secondary and primary hydroxyl groups are presented as solid and dashed lines, respectively.

The stoicheiometry of the interaction can be established by calculation of the coordination numbers, which is done by integration of the RDFs out to the first solvation shell, Figure 8(a). The coordination numbers of secondary and primary hydroxyl groups to chloride ions in the first shell are 0.85 and 0.56, respectively. If the coordination numbers are averaged over all types of hydroxyl groups, a OH···Cl hydrogen bonding stoicheiometry of 1:0.78 is obtained. This is close to the ideal 1:1 ratio expected for these systems, and agrees well with results from NMR experiments *(12)*. The slight deviation from ideality can be explained by analysis of the ion spatial distribution around the solute presented in Figure 9. The most populated cellobiose conformer observed in the simulation, which accounts for ~60% of the total, displays a lack of chloride ion density around some hydroxyl groups. Closer inspection reveals that these groups hydrogen bond intramolecularly to oxygen atoms within the carbohydrate, therefore reducing the number of OH···Cl interactions.

The spatial distribution also shows that while the anions are in close proximity to the solute, the $[C_4mim]^+$ ions lie in the periphery. This would indicate weak interactions between the cations and the sugar, in agreement with the NMR results discussed above, and can be corroborated by analysis of the RDF from the sugar oxygens to the imidazolium H-2 proton, or $g_{O\cdots H2}(r)$, and the corresponding O···H2–C2 ADF. As seen in Figure 10, there are no significant peaks above the ideal gas distribution threshold in neither the RDF nor the ADF. Contrary to what has been previously proposed *(32,33)*, this demonstrates that there are no specific interactions between the cations and the solute.

Similar analyses were carried out for the [C_2mim][O_2CMe]/cellobiose system. Once again, there is a pronounced peak in the OH···O_2CMe RDFs at 1.55 Å, Figure 11(a). Since both oxygen atoms in the anion were analysed independently, a minor peak at 3.30 Å, which corresponds to the non-interacting oxygen in each ethanoate ion, can be observed. The O–H···O_2CMe ADFs, shown in Figure 11(b), also show a maximum centred at ~170°. As was the case in the [C_4mim]Cl/cellobiose system, these distance and angle values correspond

to ideal hydrogen bonding geometry between the hydroxyl group protons and the ethanoate ions. The coordination numbers reveal that the OH···O_2CMe interactions are nearly stoicheiometric and virtually identical for primary and secondary hydroxyl groups (0.93 and 0.91, respectively). Consistent with the profile of the RDFs, there is a second plateau in the RDF integrals that corresponds to the non-interacting ethanoate oxygen atom.

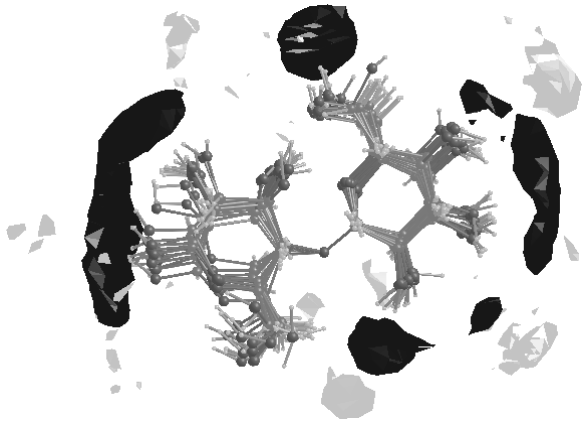

Figure 9. Spatial distribution of Cl^- (dark grey) and $[C_4mim]^+$ ions (light grey) around cellobiose in a 5 wt% $[C_4mim]Cl$/cellobiose solution. The centre of mass of the imidazolium ring was used to compute the distributions.

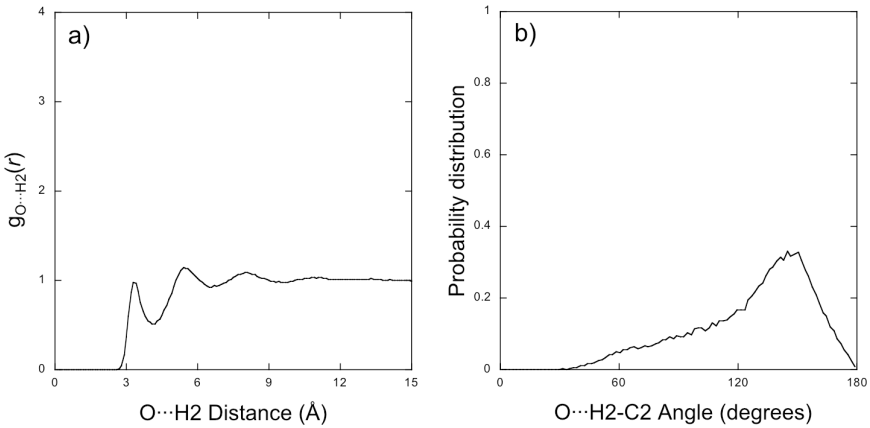

Figure 10. (a) O···H2 RDFs and (b) O···H2–C2 ADFs for the $[C_4mim]Cl$/cellobiose system

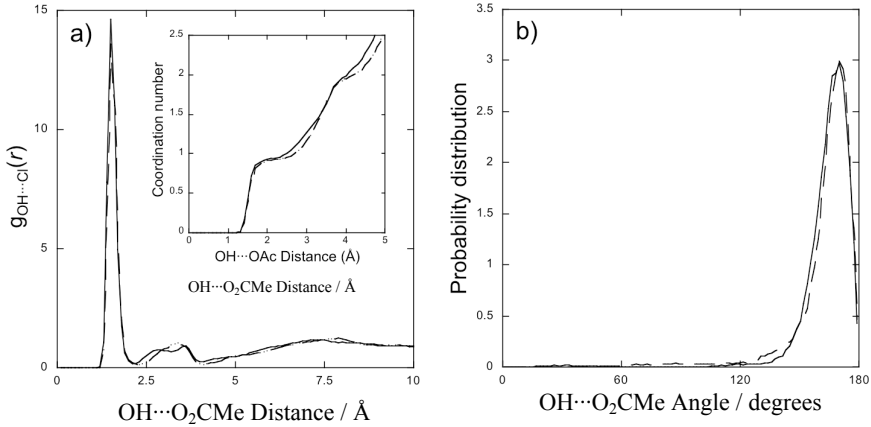

Figure 11. (a) OH···O_2CMe RDFs and coordination numbers, and (b) O-H···O_2CMe ADFs for the [C_2mim][O_2CMe]/cellobiose system. Results for secondary and primary hydroxyl groups are presented as solid and dashed lines, respectively.

The near-ideal OH···O_2CMe interaction ratio can be rationalised if the distribution of cellobiose conformers in this system is analysed. In this case, the hydroxyl groups in most of the conformer families do not display intramolecular hydrogen bonds, but instead participate in intermolecular hydrogen bonding with the ethanoate ions. Indeed, the spatial distribution of ions around the most populated cellobiose conformer shows anion density near all hydroxyl groups (Figure 12).

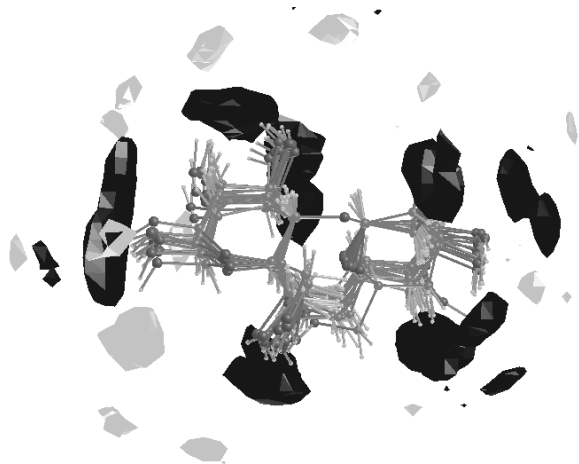

Figure 12. Spatial distribution of [O_2CMe]$^-$ (dark grey) and [C_2mim]$^+$ (light grey) ions around cellobiose in a 5 wt% [C_2mim][O_2CMe]/cellobiose solution. The centre of mass of the imidazolium ring was used to compute the distributions.

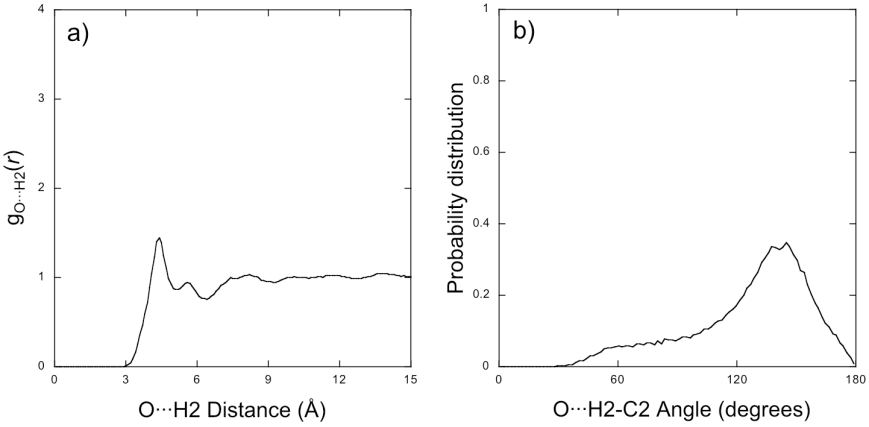

Figure 13. (a) O···H2 RDFs and (b) O···H2–C2 ADFs for the [C_2mim][O_2CMe]/cellobiose system.

By analogy to the [C_4mim]Cl/cellobiose system, further inspection of the ion spatial distribution shows limited cation density around the solute. This is also consistent with results from our NMR experiments, is again corroborated by analysis of the $g_{O\cdots H2}(r)$ and the corresponding ADF (Figure 13), and indicates a lack of specific interaction between the $[C_2mim]^+$ ion and the solute.

4. Conclusions

In summary, this chapter outlined the use of NMR spectroscopy in combination with molecular modelling simulations in the study of carbohydrate dissolution by 1,3-dialkylimidazolium ionic liquids at the molecular level. Our results conclusively show that the solvation mechanism is based on the interaction of the ionic liquid anion with the hydroxyl group protons of the sugar solute. More importantly, both experimental and theoretical methods demonstrate that the ionic liquid cation does not play a primary role in the process. Therefore, these findings suggest that while the structure of the anion is critical, that of the cation may be modified to fine tune the physicochemical properties of the ionic liquid without affecting its carbohydrate dissolving ability.

Our MD simulation analyses for the ionic liquid/sugar systems concentrated on structural parameters. These are sufficient to explain most of the experimental observations adequately in this case, but computation of dynamic properties such as ion diffusivities and correlation times of NMR-active nuclei can also be undertaken to further validate theoretical results *(6,24,34)*. Given the long simulation times required to properly reproduce the dynamics of viscous fluids such as ionic liquids, the accuracy of these estimations is generally semi-quantitative. However, they are in most cases able to reproduce

experimental trends satisfactorily and can therefore be used in the *a priori* prediction of properties of ionic liquids.

The methodology outlined here can also be applied to other systems based on ionic liquids. For example, we have employed a similar combination of NMR experiments and MD simulations to explain the effects of co-solvents on the macroscopic properties of ionic liquids *(8)*. The findings from these and other studies thus indicate that the approach should be suitable to investigate ionic liquid interactions with a wide range of materials in a variety of processes. Work in several of these areas is ongoing, and our results will be reported in due course.

Acknowledgments

Funding from the NSF CCLI-A&I and MRI programs (Grants DUE-9952264 and CHE-0420556), the Camille and Henry Dreyfus Foundation (Award TH-04-008), the H. O. West Foundation, the Merck/AAAS Undergraduate Summer Research Program, and W. R. Grace & Company is greatly acknowledged.

References

1. *Ionic Liquids IV: Not Just Solvents Anymore*, Brennecke, J. F., Rogers, R. D., Seddon, K. R., Eds. ACS Symposium Series 975, American Chemical Society: Washington, DC, 2007. See also volumes 818, 856, 901, and 902 of the same series.
2. Holbrey, J. D.; Reichert, W. M.; Nieuwenhuyzen, M.; Johnston, S.; Seddon, K. R.; Rogers, R. D. *Chem. Commun*. **2003**, 1636-1637.
3. Hardacre, C.; Holbery, J. D.; McMath, S. E. J.; Bowron, D. T.; Soper, A. K. *J. Chem. Phys*. **2003**, *118*, 273-278.
4. Dieter, K. M.; Dymek, C. J., Jr.; Heimer, N. E.; Rovang, J. W.; Wilkes, J. S. *J. Am. Chem. Soc*. **1988**, *110*, 2722-2726.
5. Bankmann, D.; Giernoth, R. *Prog. Nucl. Magn. Reson. Spectrosc*. **2007**, *51*, 63-90.
6. Margulis, C. J.; Stern, H. A.; Berne, B. J. *J. Phys. Chem. B* **2002**, *106*, 12017-12021.
7. Consorti, C. S.; Suarez, P. A. Z.; de Souza, R. F.; Burrow, R. A.; Farrar, D. H.; Lough, A. J.; Loh, W.; da Silva, L. H. M.; Dupont, J. *J. Phys. Chem. B* **2005**, *109*, 4341-4349.
8. Remsing, R. C.; Liu, Z.; Sergeyev, I.; Moyna, G. *J. Phys. Chem. B* **2008**, *112*, 7363-7369.
9. Mele, A.; Romanò, G.; Giannone, M.; Ragg, E.; Fronza, G.; Raos, G.; Marcon, V. *Angew. Chem. Int. Ed*. **2006**, *45*, 1123-1126.
10. Carper, W. R.; Wahlbeck, P. G.; Dölle, A. *J. Phys. Chem. A* **2004**, *108*, 6096-6099.
11. Remsing, R. C.; Swatloski, R. P.; Rogers, R. D.; Moyna, G. *Chem. Commun*. **2006**, 1271-1273.

12. Heimer, N. E.; Wilkes, J. S.; Wahlbeck, P. G.; Carper, W. R. *J. Phys. Chem. A* **2006**, *110*, 868-874.
13. Remsing, R. C.; Hernandez, G.; Swatloski, R. P.; Massefski, W. W.; Rogers, R. D.; Moyna, G. *J. Phys. Chem. B* **2008**, *112*, 11071-11078.
14. Noda, A.; Hayamizu, K.; Watanabe, M. *J. Phys. Chem. B* **2001**, *105*, 4603-4610.
15. Annat, G.; MacFarlane, D. R.; Forsyth, M. *J. Phys. Chem. B* **2007**, *111*, 9018-9024.
16. Moreno, M.; Castiglione, F.; Mele, A.; Pasqui, C.; Raos, G. *J. Phys. Chem. B* **2008**, *112*, 7826-7836.
17. Huddleston, J. G.; Visser, A. E.; Reichert, W. M.; Willauer, H. D.; Broker, G. A.; Rogers, R. D. *Green Chem*. **2001**, *3*, 156-164.
18. Farrar, T. C.; Becker, E. D. *Pulse and Fourier Transform NMR. Introduction to Theory and Methods*, Academic Press, New York, 1971.
19. Pelta, M. D.; Barjat, H.; Morris, G. A.; Davis, A. L.; Hammond, S. J. *Magn. Reson. Chem*. **1998**, *36*, 706-714.
20. Wider, G.; Dötsch, V.; Wüthrich, K. *J. Magn. Reson. A* **1994**, *108*, 255-258.
21. Stejskal, E. O.; Tanner, J. E. *J. Chem. Phys*. **1965**, *42*, 288-292.
22. Moore, P. B. Code for Molecular Modeling and Molecular Dynamics (CM3D). http://hydrogen.usp.edu/moore/code/cm3d.html (accessed Feb 2008).
23. Jorgensen, W. L.; Maxwell, D. S.; Tirado-Rives, J. *J. Am. Chem. Soc.* **1996**, *118*, 11225-11236.
24. Liu, Z.; Remsing, R. C.; Moore, P. B.; Moyna, G. In *Ionic Liquids: Not Just Solvents Anymore*, Brennecke, J. F., Rogers, R. D., Seddon, K. R., Eds. ACS Symposium Series, American Chemical Society: Washington, DC, 2007, pp. 335-350.
25. Darden, T. A.; York, D. M.; Pedersen, L. G. *J. Chem. Phys.* **1993**, *98*, 10089-10092.
26. Essmann, U.; Perera, L.; Berkowitz, M. L.; Darden, T.; Lee, H.; Pedersen, L. G. *J. Chem. Phys.* **1995**, *103*, 8577-8593.
27. Tuckerman, M.; Berne, B. J.; Martyna, G. *J. Chem. Phys.* **1992**, *97*, 1990-2001.
28. Hedin, N.; Furó, I.; Eriksson, P. O. *J. Phys. Chem. B* **2000**, *104*, 8544-8547.
29. Gordon, P. G.; Brouwer, D. H.; Ripmeester. J. A. *J. Phys. Chem. A* **2008**, *112*, 12527-12529.
30. Hayamizu, K.; Aihara, Y.; Nakagawa, H.; Nukuda, T.; Price, W. S. *J. Phys. Chem. B* **2004**, *108*, 19527-19532.
31. Chung, S. H.; Lopato, R.; Greenbaum, S. G.; Shirota, H.; Castner, E.W. Jr.; Wishart, J. F. *J. Phys. Chem. B* **2007**, *111*, 4885-4893.
32. Youngs, T. G. A.; Holbrey, J. D.; Deetlefs, M.; Nieuwenhuyzen, M.; Costa Gomes, M. F.; Hardacre, C. *ChemPhysChem* **2006**, *7*, 2279-2281.
33. Youngs, T. G. A.; Hardacre, C.; Holbrey, J. D. *J. Phys. Chem. B* **2007**, *111*, 13765-13774.
34. Ködderman, T.; Ludwig, R.; Paschek, D. *ChemPhysChem* **2008**, *9*, 1851-1858.